On the interrelation between nuclear dynamics and spectral line shapes in clusters

Andreas Heidenreich and Joshua Jortner
School of Chemistry, Tel Aviv University, 69978 Tel Aviv, Israel

(Received 20 November 1995; accepted 23 July 1996)

We analyze spectral absorption line shapes simulated using the molecular dynamics spectral density method. We explore three classes of line shapes: (1) the region of the 0–0 $S_0 \rightarrow S_1(\pi\pi^*)$ transition of perylene$\cdot Ar_N$ clusters, (2) the $Xe^1S_0 \rightarrow {}^3P_1$ transition of $XeAr_N$ clusters, and (3) the photoelectron spectrum of the Li_4F_4 cluster in the valence region. These spectra represent examples for weak, unresolved, and extensive vibrational progressions, which have been analyzed and assigned. Employing a simplified model for the energy gap autocorrelation function allows for an understanding of the different behaviors and for a classification of the interrelation between nuclear dynamics and spectral line shapes. With decreasing the characteristic decay time of the transition dipole autocorrelation function, the line shape passes the limiting cases of the model in the order fast modulation limit→vibrational progression limit→slow modulation limit, with the vibrational progression limit extending the limiting cases of the Kubo stochastic model of line shapes. Some simple qualitative rules have been extracted to predict the overall character of a line shape. © *1996 American Institute of Physics.* [S0021-9606(96)00241-3]

I. INTRODUCTION

The effect of nuclear dynamics on spectral line shapes is manifested by line broadening and the possible appearance of a vibrational fine structure. The semiclassical molecular dynamics spectral density method of Fried and Mukamel[1–7] is an appealing tool to simulate temperature-dependent spectral line shapes, as the simulations are simple to perform and are not limited to a few vibrational degrees of freedom, unlike wave packet dynamics simulations.

So far the spectral density method has been applied to the $S_0 \rightarrow S_1$ absorption spectra of van der Waals heteroclusters consisting of an aromatic molecule and rare gas atoms,[1,2,8–14] to the ${}^1S_0 \rightarrow {}^3P_1$ absorption spectra of $XeAr_N$ heteroclusters[15] and to the photoelectron spectrum of the Li_4F_4 cubic cluster.[16] Whenever the simulated homogeneous line shapes could be compared with the experimental ones, which was the case for some small aromatic molecule–rare gas heteroclusters[8,9,12] and $XeAr_N$ heteroclusters,[15,17–20] where the experimental line shape was not disturbed by inhomogeneous line broadening, the simulated homogeneous linewidths as well as the overall line shape were in close agreement with the experiment. Although the number of applications of the spectral density method is still small, a comparative analysis of the spectra and a classification of the interrelation between nuclear dynamics and spectral line shapes is already possible at this stage. This is the subject of the present paper.

II. THE SPECTRAL DENSITY METHOD

In the spectral density method,[1–7] the homogeneous absorption line shape $L(\omega)$ is expressed by the Fourier transform of the time-dependent transition dipole autocorrelation function $I(t)$

$$L(\omega) = \frac{1}{\pi} \mathrm{Re} \int_0^\infty dt \, \exp(-i\omega t) I(t). \tag{1}$$

At present the spectral density method is limited to electronic two-level systems. The decay of the transition dipole autocorrelation function is determined by the nuclear dynamics. The basic idea is to treat the nuclear dynamics classically and explicitly only on one of the two potential energy hypersurfaces, in our case always on the hypersurface of the ground electronic state. The influence of the second (excited state) hypersurface on the nuclear dynamics and thus on $I(t)$ is treated by perturbation theory. The perturbation is given by the different shape of this second hypersurface, which would alter the trajectory, if the dynamics took place there.[21–24] As a consequence of the Condon approximation, the central input quantity is the time-dependent energy gap function $U(t)$, the vertical excitation energy along the classical trajectory on the ground electronic state potential energy hypersurface.

The transition dipole autocorrelation function is approximated by a second-order cumulant expansion, resulting in

$$I(t) = \exp(-g(t)), \tag{2}$$

where

$$g(t) = \int_0^t dt_1 \int_0^{t_1} dt_2 \; J_{\mathrm{SC}}(t_2) \tag{3}$$

is the two-time integral of the semiclassical energy gap autocorrelation function. $J_{\mathrm{SC}}(t)$ is related to the classical energy gap autocorrelation function

$$J(t) = \langle (U(0) - \langle U \rangle)(U(t) - \langle U \rangle) \rangle \tag{4}$$

in the frequency space by a quantum correction

$$J_{\mathrm{SC}}(\omega) = \left[1 + \tanh\left(\frac{\hbar\omega}{2k_B T} \right) \right] J(\omega). \tag{5}$$

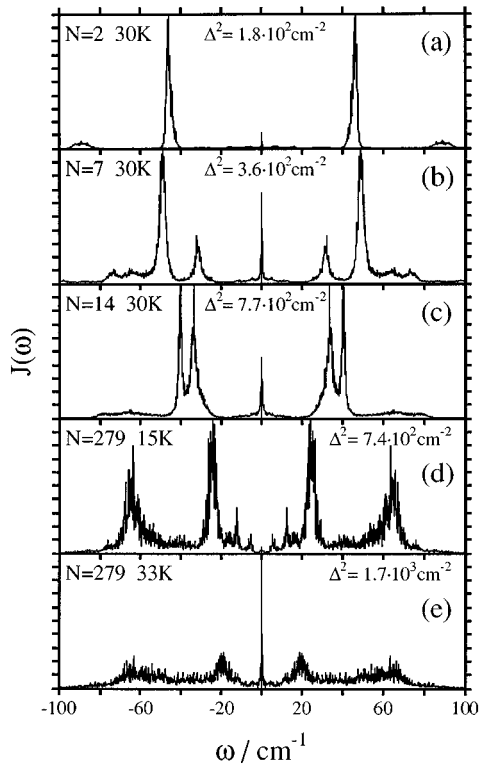

FIG. 1. The classical energy gap power spectra of various perylene·Ar_N heteroclusters. (a)–(c) The power spectra of the $N=2$, 7, and 14 clusters at 30 K, (d)–(e) The power spectra of the $N=279$ cluster at 15 and 33 K. The total dispersion Δ^2 is indicated in each panel.

Some typical examples of the energy gap autocorrelation function Fourier transform $J(\omega)$, e.g., the classical power spectrum, are presented in Fig. 1 for perylene·Ar_N heteroclusters. In the next section, the power spectra are the starting point for a simplified model of the spectral line shapes.

The consequence of performing the dynamics only on the ground state hypersurface is that the level spacing of a vibrational progression corresponds to the ground state. However, the Franck–Condon envelope is sampled correctly within the classical approximation of the probability density of the nuclei. Performing the dynamics only on one hypersurface can be also of advantage, when explicit dynamics on both hypersurfaces is computationally too demanding, in particular in *ab initio* molecular dynamics simulations evaluating the energies and energy gradients at each molecular dynamics step directly by quantum chemical calculations. Electronically excited states mostly require an excessive treatment of electron correlation. In this context it should be emphasized that the spectral density method does not require excited state energy gradients. Moreover, $U(t)$ need not be evaluated at every molecular dynamics time step, as the relevant sampling interval is determined by the maximum vibrational frequency of the system.

The spectral density method allows for an incorporation of inhomogeneous broadening. Although inhomogeneous broadening[25,26] is not the subject of this paper, we address this point here in the context of averaging procedures applied to the derivation of homogeneous line shapes. Inhomogeneous broadening arises from different microenvironments (cluster isomers), which are experienced by the chromophore. In the spectral density method, single-trajectory spectra (''subspectra'') are homogeneous on principle. Microenvironments, which interconvert in the course of a trajectory (e.g., in a cluster isomerization), must be considered as a new single (unified) microenvironment (''communicating microenvironments'').[14,27,28] In the spectral density method, inhomogeneous broadening is simulated by a superposition of homogeneous single-trajectory spectra, where the initial conditions for each trajectory are chosen, in the ideal case, according to the statistical abundance of the microenvironments (cluster isomers) under experimental conditions. Trajectories of different microenvironments have different average energy gap values $\langle U \rangle$ and therefore different band positions. Consequently, a superposition of these subspectra leads to inhomogeneous line broadening. Obviously, due to incomplete sampling (too short simulation times), the $\langle U \rangle$ values as well as the overall line shapes of different trajectories differ in practical simulations, even if the microenvironment is expected to be the same (no cluster isomers). This ''artificial inhomogeneous broadening'' spoils the line shape in those cases where the homogeneous linewidths become as small as the differences in the sampled $\langle U \rangle$ values (in particular for small aromatic molecule rare gas heteroclusters like perylene·Ar_2). Since even a substantial enhancement of the simulation times did not lead to a convergence in these pathological cases, we calculated the homogeneous line shapes from the power spectra averaged over several trajectories. This procedure[14] was applied to all multitrajectory spectra presented in this paper (perylene·Ar_N and $XeAr_N$ clusters).

III. A SIMPLIFIED LINE SHAPE MODEL

In the classical power spectrum each peak j, termed an oscillator, can be approximated by a Lorentzian

$$J_j(\omega) = \frac{2\Delta_j^2 \gamma_j}{\gamma_j^2 + (\omega - \omega_j)^2}, \tag{6}$$

with a peak maximum ω_j (the oscillator frequency), the dispersion Δ_j^2 (the area under the Lorentzian) and the half width at half maximum γ_j . Δ_j^2 expresses the difference of the shape of the ground and excited electronic state potential energy hypersurfaces in the region accessible by the classical trajectories. γ_j reflects the intracluster vibrational energy redistribution (IVR).[29–31] The correspondence of the γ_j parameter to quantum mechanical quantities has not been investigated yet. The model of the power spectrum allows us to derive an analytical expression for the line shape and to discuss the dependence of the line shape as a function of a few parameters.

The classical power spectra $J(\omega)$ are symmetric with respect to $\omega=0$. The quantum correction factor $\kappa_j = 1 + \tanh(\hbar\omega_j/2k_BT)$ removes this symmetry, enhancing the dispersion of the oscillators at positive frequencies at the cost

of the corresponding oscillators at negative frequencies, where the total dispersion remains constant. The semiclassical function $J_{j,\mathrm{SC}}(\omega)$ reads

$$J_{j,\mathrm{SC}}(\omega)=\frac{2\kappa_j\Delta_j^2\gamma_j}{\gamma_j^2+(\omega-\omega_j)^2}. \tag{7}$$

The semiclassical energy gap autocorrelation function $J_{j,\mathrm{SC}}(t)$ is

$$J_{j,\mathrm{SC}}(t)=\kappa_j\Delta_j^2\ \exp(i\omega_j t)\exp(-\gamma_j|t|) \tag{8}$$

and the corresponding $\exp(-g_j)$ function

$$\begin{aligned}\exp(-g_j)=&\exp\left(\frac{\kappa_j\Delta_j^2(\gamma_j+i\omega_j)^2}{(\gamma_j^2+\omega_j^2)^2}\right)\\&\cdot\ \exp\left(-\frac{\kappa_j\Delta_j^2(\gamma_j+i\omega_j)}{\gamma_j^2+\omega_j^2}\,t\right)\\&\cdot\exp\left(-\frac{\kappa_j\Delta_j^2(\gamma_j+i\omega_j)^2}{(\gamma_j^2+\omega_j^2)^2}\right.\\&\left.\times\exp(-\gamma_j|t|)\exp(i\omega_j t)\right).\end{aligned} \tag{9}$$

Now we are able to discuss the effect of a single oscillator on the line shape. The first exponential factor in Eq. (9) is constant in t and need not be further considered, because it affects only the absolute intensity of the line shape. The second exponential factor in Eq. (9) manifests two effects. The real part is responsible for line broadening. Without the third factor of the e^{-g} function, the line shape would always be Lorentzian with a linewidth of $2\kappa_j\Delta_j^2\gamma_j/(\gamma_j^2+\omega_j^2)$. The imaginary part shifts the line shape by $\kappa_j\Delta_j^2\omega_j/(\gamma_j^2+\omega_j^2)$ with respect to $\langle U\rangle$, the center of the spectrum. This frequency shift is partly compensated by the corresponding oscillator at $-\omega_j$. To analyze the third factor in Eq. (9), we expand the outer exponential into a Taylor series

$$\begin{aligned}\sum_{n=0}^{\infty}&\left[\frac{1}{n!}\left(\frac{-\kappa_j\Delta_j^2(\gamma_j+i\omega_j)^2}{(\gamma_j^2+\omega_j^2)^2}\right)^n\right.\\&\left.\times\exp(in\omega_j t)\exp(-n\gamma_j|t|)\right].\end{aligned} \tag{10}$$

Expression (10) can give rise to a vibrational progression with a Poissonian intensity distribution, where the nth term corresponds to the $m\rightarrow m+n$ transitions for oscillators at positive frequencies and to the $m\rightarrow m-n$ transitions for oscillators at negative frequencies, e.g., the $n=0$ term comprises the $0\rightarrow0$, $1\rightarrow1$, $2\rightarrow2$, etc., vibronic transitions. For $\omega_j\gg\gamma_j$, which is always the case except for the soft modes at $\omega_j\approx0$, the relative intensities of the vibronic transitions of the progression are given by

$$\frac{1}{n!}\left(\frac{\kappa_j\Delta_j^2}{\omega_j^2}\right)^n. \tag{11}$$

Whether such a progression can be observed is strongly dependent on the ratio of the parameters ω_j, Δ_j, and γ_j. First, the progression assumes only an appreciable extension for ratios $\kappa_j\Delta_j^2/\omega_j^2\geqslant1$, as is evident from expression (11). One consequence is that a $m\rightarrow m-n$ progression is always less extensive than the corresponding $m\rightarrow m+n$ progression, due to the smaller κ values of negative frequencies. For $\kappa_j\Delta_j^2/\omega_j^2\ll1$, which is the case when the two potential hypersurfaces are very similar, the $n=0$ transition is the dominating spectral feature. Second, the appearance of a vibrational progression depends on the decay rate of the e^{-g} function. For $\kappa_j\Delta_j^2/\omega_j^2\geqslant1$, this factor represents the major contribution to the decay of the e^{-g} function. If the e^{-g} function decays too fast, the vibronic bands coalesce to a single broad Gaussian, which spans the entire progression, with a FWHM (full width at half maximum) of $\Gamma=2(2\ln2)^{1/2}\Delta_j$. This is the slow modulation limit. We will now discuss the limiting cases of the line shape model more systematically.

A. The fast modulation limit

The fast modulation limit was originally formulated for $\omega_j=0$ (the Kubo limit).[32,33] The Kubo fast modulation limit applies, if the term $\exp(-\gamma_j|t|)$ can be neglected in the g function (long time approximation). This approximation is valid for $\gamma_j\gg\Delta_j$. Then the line shape is Lorentzian with a FWHM of $\Gamma=2\Delta_j^2/\gamma_j$. A consequent extension to finite frequencies requires that the term $\exp(i\omega_j\tau)\cdot\exp(-\gamma_j|t|)$ in the third term of the e^{-g} function, Eq. (9), becomes negligible. This is the case if $\gamma_j^2+\omega_j^2\gg\kappa_j\Delta_j^2$. Then the spectrum exhibits only a Lorentzian $n=0$ band with a FWHM

$$\Gamma_{n=0}=2\,\frac{\kappa_j\Delta_j^2\gamma_j}{\gamma_j^2+\omega_j^2}. \tag{12}$$

Since the decay of the $\exp(-g_j)$ function is exclusively determined by the second term of Eq. (9), the exponential decay time τ_j is given by

$$\tau_j=\frac{\gamma_j^2+\omega_j^2}{\kappa_j\Delta_j^2\gamma_j}. \tag{13}$$

In the general case τ_j is not given by such a simple expression, so that we determined τ_j by a numerical inspection of the $\exp(-g_j)$ function, when, in general, the oscillatory function drops *permanently* below $1/e$. Using τ_j, Eq. (13), the criterion for the fast modulation limit can be recast as $\gamma_j\tau_j\gg1$.

B. The slow modulation limit

The character of the $\exp(-g_j)$ function is mainly determined by its behavior up to τ_j. In the slow modulation limit, the g function is quadratic in t. A quadratic expansion of $\exp(i\omega_j t)$ and $\exp(-\gamma_j|t|)$ occurring in the g function requires (1) $\omega_j\tau_j\leqslant\pi/2$ and (2) $\gamma_j\tau_j<1$. Both criteria can be met by finite frequencies and by the soft mode $\omega_j\approx0$ (Kubo limit). In the latter case, condition (1) always applies and condition (2) simplifies to $\gamma_j/\Delta_j<1$. For finite frequency components, the first condition is more demanding. The ideal case of the slow modulation limit is given by $\omega_j\tau_j\ll\pi/2$ and $\gamma_j\tau_j\ll1$. The corresponding parameter constellation is $\omega_j,\gamma_j\ll\Delta_j$.

C. The case of a vibrational progression

A vibrational progression may be expected, if (1) $\omega_j\tau_j \geqslant 2\pi$ and (2) $\gamma_j\tau_j < 1$. Condition (1) means that the g function must be able to perform an oscillation within the period τ_j. In practical model calculations for one oscillator, however, it turned out that some vibrational fine structure starts to appear already for $\omega_j\tau_j > \pi/2$, indicating that the decay of the $\exp(-g_j)$ function is not complete at τ_j. In other words, the range $\pi/2 < \omega_j\tau_j < 2\pi$ represents a situation where the Gaussian line shape gradually evolves into a vibrational progression.[21] In the ideal case, $\omega_j\tau_j \gg 2\pi$ and $\gamma_j\tau_j \ll 1$, which corresponds to the case of a well resolved and extensive progression, the relative intensities are given by expression (11), and the line shapes of the vibronic transitions are Lorentzian, with a FWHM of

$$\Gamma_n = 2\left(\frac{\kappa_j\Delta_j^2\gamma_j}{\omega_j^2} + n\gamma_j\right). \tag{14}$$

Equation (14) applies to both $m \rightarrow m+n$ and $m \rightarrow m-n$ transitions. Parameter constellations for a resolved and extensive progression are $\gamma_j \ll \omega_j \approx \Delta_j$ and in principle also $\gamma_j \ll \omega_j \ll \Delta_j$. However, as we shall see in Sec. IV B, the latter parameter constellation contains the danger of a coalescence to a broad Gaussian (slow modulation limit).

In previous line shape analysis we made use of models, in which an exponential decaying cosine function,[14] a heuristic description of a damped oscillator motion

$$J_j(t) = \Delta_j^2 \cos(\omega_j t)\exp(-\gamma_j|t|), \tag{15}$$

or the damped oscillator function itself[34–37]

$$J_j(t) = \Delta_j^2\left(\cos(\omega_j t) + \frac{\gamma_j}{\omega_j}\sin(\omega_j t)\right)e^{-\gamma_j|t|} \tag{16}$$

was taken for the energy gap autocorrelation function of a single oscillator. In both models the quantum correction factor is disregarded. Especially Eq. (16) seems to be appealing, as it relates the damping of the autocorrelation function closer to the physical picture of the damping of the vibration itself due to intracluster vibrational energy redistribution. However, since the line shape analysis of the present paper is not limited to the $n=0$ band, a model, which incorporates the quantum correction factor, is more suitable.

D. Several oscillators

When *several oscillators* are present, the total e^{-g} function is given by

$$\exp(-g) = \prod_j \exp(-g_j). \tag{17}$$

If all oscillators were in the fast modulation limit, the total $1/e$ time τ_{tot} is

$$\tau_{\text{tot}} = \left[\sum_j (\tau_j^{-1})\right]^{-1}. \tag{18}$$

Although Eq. (18) does not apply *quantitatively* in the general case, it shows *qualitatively* that an oscillator of a sufficiently short τ_j causes the entire e^{-g} function to correspond to the slow modulation limit, even if all the other oscillators do not. The conditions for the slow modulation limit, a vibrational progression and the fast modulation limit, are analogous to the single oscillator case with the difference that the conditions must now be applied to τ_{tot}. In analogy to the τ_j, τ_{tot} was obtained by a numerical inspection of the total e^{-g} function rather than by Eq. (18).

In general, the contributions of the distinct oscillators to the linewidth are not additive. Some cases, where the relation of the total linewidth to the individual contributions is simple, are (i) If the entire e^{-g} function is in the fast modulation limit, with the individual linewidths being additive. (ii) One oscillator causes a vibrational progression, while all the other oscillators are in the fast modulation limit. As in case (i), the contributions are additive. (iii) The entire e^{-g} function is in the slow modulation limit. Then the linewidth is given by 2.355Δ; Δ^2 being the sum of the dispersions of all oscillators. (iv) m oscillators are in the progression limit. Then the linewidth of a vibronic transition $n_1 n_2 \cdots n_m$ is obtained by the sum of the linewidths of the individual vibronic transitions, $\Gamma(n_1,n_2,..,n_m) = \Gamma(n_1)+\Gamma(n_2)+\cdots+\Gamma(n_m)$; where the $\Gamma(n_i)$ are given by Eq. (14). (v) One oscillator gives rise to a well resolved progression, one or several oscillators are in the slow modulation limit, without driving the entire e^{-g} function into the slow modulation limit. Then the resulting line shape exhibits a vibrational progression, where each vibronic band is Gaussian.

IV. ANALYSIS OF SOME SPECTRA

A. The $S_0 \rightarrow S_1(\pi\pi^*)$ electronic transition of aromatic molecule–rare gas heteroclusters

In the first example we consider uv/vis spectra of aromatic-molecule (perylene) rare-gas (argon) heteroclusters in the spectral region of the electronic origin of the $S_0 \rightarrow S_1(\pi\pi^*)$ transition of the aromatic molecule. Figure 2 shows five simulated homogeneous absorption line shapes of a small, of two medium sized and of a large perylene$\cdot$Ar$_N$ cluster ($N=2,7,14,279$, see Fig. 3). The line shapes for the $N=2$, 7, and 14 clusters were simulated at 30 K, the $N=279$ cluster at 15 and 33 K. The line shapes are determined by the *inter*molecular motions only, as the underlying molecular dynamics (MD) simulations were carried out for a rigid but not space-fixed perylene molecule.[13,14] Lennard-Jones 6-12 potentials have been employed for the intermolecular interactions, with different parameter sets[14] for the ground and for the electronically excited state of the perylene molecule. The homogeneous line shapes were calculated from the averaged power spectra, Fig. 1. The extracted parameter sets $\{\omega_j, \Delta_j, \gamma_j\}$ as well as the calculated quantum correction factors κ_j are listed in Table I. The averaging of the power spectra was carried out over 50 trajectories for the $N=2$, 7, and 14 clusters and over ten trajectories for the $N=279$ cluster. Each trajectory had a temporal length of 340 ps and a sampling interval of 80 fs, resulting in a spectral resolution

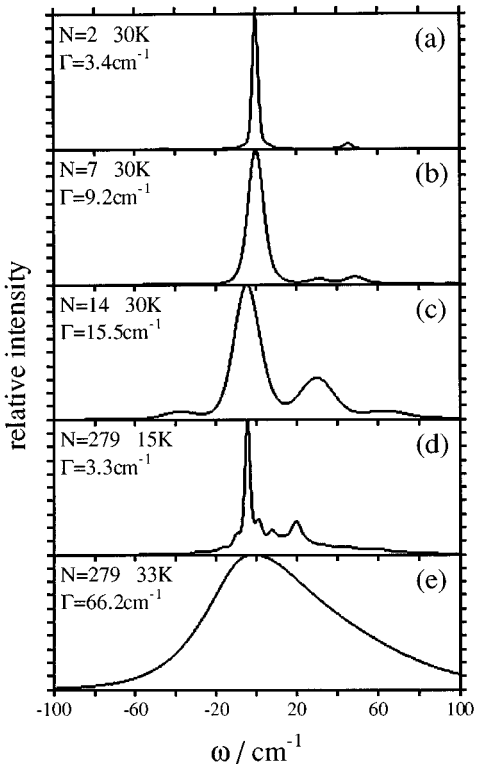

FIG. 2. The simulated optical line shapes of various perylene·Ar_N heteroclusters using the spectral density method. (a)–(c) The spectra of the $N=2$, 7, and 14 clusters at 30 K, (d)–(e) the spectra of the $N=279$ cluster at 15 and 33 K. The center of each spectrum constitutes the origin of the energy axis, disregarding the different average energy gap values $\langle U \rangle$.

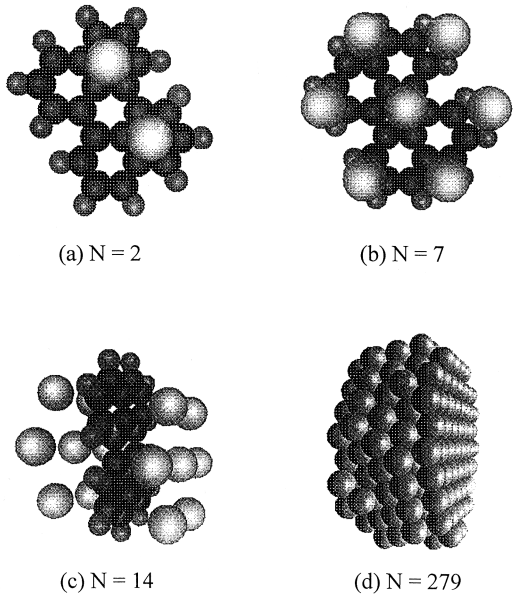

FIG. 3. Images of the perylene·Ar_N clusters. The depicted nuclear configurations correspond to local minima on the potential energy hypersurfaces; their possible global minimum character has not been examined. For the $N=279$ cluster, the van der Waals radii of the Ar atoms have been used to bring the overall shape of the cluster into prominence. The view is almost parallel to the five Ar layers. The perylene molecule is completely covered by Ar atoms and is therefore invisible.

of 0.1 cm^{-1} and a maximum frequency of 200 cm^{-1}. The main spectral features and their assignments are summarized in Table II.

The clusters are imaged in Fig. 3. In the $N=2,7$ clusters, the Ar atoms are located on one side of the molecular plane [shorthand notations: (2|0) and (7|0), respectively], in the $N=14$ cluster 7 Ar atoms are placed on either side [(7|7) isomer]. The Ar dimer of the $N=2$ cluster, in Fig. 3(a) localized on two six rings of the perylene surface, can move freely on the perylene surface already at temperatures much lower than the simulation temperature of 30 K. In the $N=7$ and $N=14$ clusters, Figs. 3(b) and 3(c), each of the Ar_7 subunits (''adclusters'') are in one layer, forming filled hexagons on the molecular surface. In the perylene·Ar_{279} cluster, Fig. 3(d), the perylene molecule is placed in the central 111 layer of a fcc lattice of Ar atoms with two layers of Ar atoms on both sides of the aromatic molecule surface. The perylene molecule replaces 16 Ar atoms of the central Ar layer. The first shell around the perylene molecule consists of 43 Ar atoms, covering also the peripheral H atoms.

The most intense spectral feature (Fig. 2) is the $n=0$ (0–0) band, which is broadened and redshifted compared to the 0–0 band of the bare molecule. The redshift, as well as the total dispersion, increases monotonously with the number of Ar atoms in the first layer; additional Ar atoms in higher layers almost do not contribute. Aside from the $n=0$ band, the optical spectra show some additional fine structure. The line shape of the perylene·Ar_2 cluster, Fig. 2(a), exhibits a weak vibronic band at 46 cm^{-1} relative to its $n=0$ band. The vibronic band has been assigned to the $n=1$ vibronic transition of the vibration of the Ar atoms perpendicular to the aromatic molecule surface (''z vibration''). Vibronic bands around 40 cm^{-1} are characteristic for aromatic-molecule–Ar heteroclusters and were also found in the experimental spectra of tetracene·Ar_N[38] and dichloroanthracene·Ar_N[39] heteroclusters. The power spectrum of the (2|0) cluster, Fig. 1(a), exhibits its most intense oscillators at ± 46 cm^{-1}. The intensity of the $n=1$ transition relative to the intensity of the $n=0$ band can be obtained from expression (11) as $\kappa_j \Delta_j^2/\omega_j^2$. From the parameters listed in Table I one obtains a relative intensity of 0.059 of the $n=1$ transition, in close agreement with the value of 0.061 of the simulated line shape. Higher vibronic transitions are, according to expression (11), expected to be much weaker and therefore cannot be observed in the simulated spectrum.

The line shape of the (7|0) cluster, Fig. 2(b), shows two vibronic bands at 31 and 49 cm^{-1} relative to the $n=0$ band, with relative intensities of 0.054 and 0.073. The corresponding power spectrum, Fig. 1(b), shows two oscillators at these frequencies. On the basis of the intensities, 0.051 and 0.067, calculated by expression (11) and the extracted parameter sets of the power spectrum, both bands must be assigned to $n=1$ transitions. Looking at the Fourier transforms of the velocity components of the Ar atoms projected on the perylene surface, the underlying vibrations have mainly a z character. Moreover, the coefficients of the velocity Fourier transform allow for the determination of the phases of the Ar atoms.[40] The oscillator at higher frequency represents the

TABLE I. The parametrization of the power spectra of perylene·Ar_N clusters and some derived quantities.

Cluster	Osc. j	ω_j (cm^{-1})	Δ_j^2 (cm^{-2})	γ_j (cm^{-1})	κ_j	$\kappa_j\Delta_j^2/\omega_j^2$	τ_j (ps)	$\omega_j\tau_j$	$\gamma_j\tau_j$	$\omega_j\tau_{tot}$	$\gamma_j\tau_{tot}$	Γ_{slow} (cm^{-1})[b]	Γ_{fast} (cm^{-1})[c]	Γ_j (cm^{-1})[d]
$N=2$	1	0	1.7	0.2	1		5.92	0	0.21	0	0.19	3.1	17.8	2.9
$T=30$ K	2	7.0	1.5	1.0	1.17	$3.6\cdot10^{-2}$	150	197	28	6.8	0.97	3.1	0.07	0.07
	3	−7.0	1.5	1.0	0.83	$2.5\cdot10^{-2}$	210	276	40	6.8	0.97	2.6	0.05	0.05
	4	46.2	69.7	0.9	1.80	$5.9\cdot10^{-2}$	98.7	859	17	45	0.88	26.4	0.11	0.10
	5	−46.2	69.7	0.9	0.20	$6.5\cdot10^{-3}$	912	7940	155	45	0.88	8.7	0.01	0.02
	6	88.9	11.5	2.6	1.97	$2.9\cdot10^{-3}$	361	6040	173	87	2.5	15.9	0.03	0.02
	Total		179.5[a]				5.17					31.6		3.1[e]
$N=7$	1	0	17.5	1.1	1		1.83	0	0.37	0	0.32	9.9	32.4	9.0
$T=30$ K	2	31.8	31.6	1.8	1.64	$5.1\cdot10^{-2}$	58.9	353	20	9.5	0.53	16.9	0.18	0.17
	3	−31.8	31.6	1.8	0.36	$1.1\cdot10^{-2}$	273	1640	91	9.5	0.53	7.9	0.04	0.05
	4	49.4	88.9	1.3	1.83	$6.7\cdot10^{-2}$	58.9	550	15	15	0.40	30.0	0.18	0.17
	5	−49.4	88.9	1.3	0.17	$6.2\cdot10^{-3}$	636	5920	160	15	0.40	9.2	0.02	0.02
	Total		360.9[a]				1.58					44.7		9.2[e]
$N=14$	1	0	42.0	1.3	1		1.17	0	0.29	0	0.23	15.3	63.2	14.1
$T=30$ K	2	34.1	210.0	2.0	1.67	0.30	8.30	53	3.1	5.9	0.34	44.1	1.18	1.20
	3	−34.1	210.0	2.0	0.33	$6.0\cdot10^{-2}$	45.3	290	17	5.9	0.34	19.5	0.23	0.22
	4	40.5	109.4	0.8	1.75	0.12	53.2	410	8.3	7.0	0.14	32.6	0.19	0.20
	5	−40.5	109.4	0.8	0.25	$1.7\cdot10^{-2}$	375	2860	59	7.0	0.14	12.3	0.03	0.02
	Total		770.5[a]				0.917					65.4		15.4[e]
$N=279$	1	0	2.6	1.0	1		5.50	0	1.08	0	0.32	3.8	5.0	2.9
$T=15$ K	2	5.8	7.0	0.7	1.26	0.27	27.5	29	3.4	1.7	0.20	7.0	0.34	0.34
	3	−5.8	7.0	0.7	0.74	0.16	41.9	44	5.2	1.7	0.20	5.4	0.20	0.20
	4	12.6	16.7	0.7	1.52	0.16	38.0	89	5.2	3.8	0.22	11.9	0.23	0.22
	5	−12.6	16.7	0.7	0.48	$5.0\cdot10^{-2}$	137	320	19	3.8	0.22	6.6	$7.1\cdot10^{-2}$	0.10
	6	+24.7	128.4	1.5	1.82	0.38	8.22	38	2.4	7.5	0.47	36.0	1.17	1.17
	7	−24.7	128.4	1.5	0.18	$3.9\cdot10^{-2}$	86.1	400	25	7.5	0.47	11.4	0.12	0.12
	8	63.8	156.9	3.8	1.99	$7.7\cdot10^{-2}$	17.9	210	13	19	1.2	41.6	0.58	0.59
	Total		739[a]				1.61					64.0		6.1[e]
$N=279$	1	0	66.9	0.24	1		0.92	0	$4.1\cdot10^{-2}$	0	$1.0\cdot10^{-2}$	19.3	558	19.1
$T=33$ K	2	21.4	333	5.4	1.43	1.04	0.79	3.2	0.80	0.90	0.23	51.4	10.5	32.6
	3	−21.4	333	5.4	0.57	0.41	2.29	9.2	2.3	0.90	0.23	32.4	4.2	4.3
	4	59.9	404	8.1	1.86	0.21	3.02	34	4.6	2.5	0.34	64.6	3.3	3.4
	5	−59.9	404	8.1	0.14	$1.6\cdot10^{-2}$	42.1	470	64	2.5	0.34	17.6	0.25	0.24
	Total		1680[a]				0.23					96.5		61.1[e]

[a]The total dispersion Δ_{total}^2 of the power spectrum. The value always exceeds the sum of the dispersions of all oscillators listed in the table, since only the most important oscillators have been parametrized.

[b]Homogeneous linewidths in the slow modulation limit, $\Gamma_{slow}=2.355\kappa_j^{1/2}\Delta_j$. The values ''total'' have been calculated from the total dispersions (a), $\Gamma_{slow}=2.355\Delta_{total}$.

[c]Homogeneous linewidths in the fast modulation limit, Eq. (12).

[d]Homogeneous linewidths of the $n=0$ transitions obtained by inspection of the individual line shapes of the simplified line shape model, Eq. (9).

[e]The total homogeneous linewidths of the $n=0$ transitions obtained from the total $\exp(-g)$ function, Eq. (17).

in-phase vibration of the Ar atoms, while the phase shift of some Ar atoms tends to 180° at the lower frequency (antiphase vibration). The velocity autocorrelation Fourier transform contains further oscillators, which have no notable intensities in the energy gap power spectrum.

The (7|7) cluster could be considered, at a first sight, as a doubled (7|0) cluster. Indeed, the average energy gap value of -412 cm^{-1} is almost twice as high as the corresponding value, -208 cm^{-1}, of the (7|0) cluster. However, the line shape of the (7|7) cluster, Fig. 2(c), is quite different from that of the (7|0) cluster. The (7|7) cluster exhibits a much stronger progression consisting of the $n=-1$, the $n=1$, and the $n=2$ transition, at -33, 35, and 70 cm^{-1} with respect to the $n=0$ band and relative intensities of 0.07, 0.4, and 0.09, respectively. One reason for the stronger progression is the larger number of Ar atoms contributing to the dispersion. The other reason is the smaller frequency separation of the most intense oscillators of the power spectrum. These oscillators, located at 34 and 41 cm^{-1}, represent the antiphase and the in-phase z vibration of the Ar atoms, in analogy to the (7|0) cluster. Due to the smaller frequency separation, the dispersions of both oscillators can be cumulative. The smaller frequency separation is obviously due to the different coupling of the motion of the rigid, but not space-fixed, perylene molecule relative to the two Ar_7 adclusters. In conclusion, the (7|7) cluster is dynamically not simply a doubled (7|0) cluster. While previous simulations could successfully describe spectral shifts keeping the aromatic molecule space fixed,[41,42] such a treatment is apparently improper to account for the intermolecular vibrational fine structure. However, a complete modeling of the dynamical behavior of perylene·Ar_N clusters should also incorporate the low-frequency intramolecular butterfly motions of the perylene molecule.[43–47]

The energy gap power spectra and the optical line shapes of the $N=279$ cluster at 15 and 33 K are presented in Figs.

TABLE II. The simulated homogeneous line shapes of perylene·Ar_N heteroclusters.

Cluster size N, Temperature, δ[a]	ω (cm^{-1})[b]	Rel. Int.[c]	Rel. Int.[d]	Γ (cm^{-1})[e]	Assignment
$N=2$, 30 K,	0	$\equiv 1$	1.00	3.4	$n=0$
-88 cm^{-1}	46	0.061	0.059	4.8	$z,n=1$
$N=7$, 30 K,	0	$\equiv 1$	1.00	9.2	$n=0$
-207 cm^{-1}	31	0.054	0.051		Antiphase $z,n=1$
	49	0.073	0.067		In-phase $z,n=1$
$N=14$, 30 K,	-33	0.074	0.076		In-phase+antiphase $z,n=1$
-411 cm^{-1}	0	$\equiv 1$	1.00	15.5	$n=0$
	35	0.38	0.42	21.1	In-phase+antiphase $z,n=1$
	70	0.094	0.052		In-phase+antiphase $z,n=2$
$N=279$, 15 K,	-12	(Shoulder)	0.050		$xy,n=-1$
-835 cm^{-1}	-5	(Shoulder)	0.15		$xy,n=-1$
	0	$\equiv 1$	1.00	3.3	$n=0$
	5		0.26		$xy,n=1$
	12		0.16		$xy,n=1$
	24		0.38		$z,n=1$
$N=279$, 33 K,	0			66.2	
-824 cm^{-1}					

[a]δ: position of the electronic origin ($n=0$ band), being identical with the spectral shift of the cluster.
[b]Relative position of the vibronic band with respect to the position δ of the $n=0$ band.
[c]Relative intensity of the vibronic band.
[d]Relative intensity of the vibronic band expected according to expression (11).
[e]Simulated homogeneous linewidth.

1(d)–1(e) and 2(d)–2(e). At 15 K the $n=0$ band is sufficiently narrow, so that a resolved vibrational fine structure can be observed. The vibronic bands at 6 and 12 cm^{-1} are assigned to xy vibrations of the Ar atoms (x,y: long and short molecular axis, respectively), the band at 24 cm^{-1} is a z vibration. The energy gap power spectrum contains another strong z vibration at 64 cm^{-1}, which does not appear in the optical spectrum due to the smaller Δ/ω ratio. 75% of the dispersion of the z vibrations is caused by ten first-shell Ar atoms, five below and five above the central part of the perylene surface, while for the xy vibrations also peripheral first-shell atoms are important. Above 25 K the vibronic structure coalesces to a single broad band [Fig. 2(e)].

Proceeding to the analysis in terms of the simplified line shape model, three issues are of particular interest: (i) the characterization of the individual oscillators (fast and slow modulation limit, vibrational progression), (ii) the combined action of all oscillators with respect to the overall line shape, and (iii) the line broadening mechanism.

The extracted parameters $\{\omega_j,\Delta_j,\gamma_j\}$ of the power spectra, Table I, have been used to perform model calculations for the $\exp(-g_j)$ functions, Eq. (9), and for the line shapes of the individual oscillators, as well as for the total $\exp(-g)$ function, Eq. (17), and the corresponding line shape. From these model calculations the exponential decay times τ_j of the $\exp(-g_j)$ functions and the linewidths Γ_j have been obtained. These and other quantities characterizing the oscillators are also listed in Table I. Two examples of model calculations for the $N=14$ and the $N=279$ cluster are presented in Figs. 4 and 5.

From the $\omega_j\tau_j$ and $\gamma_j\tau_j$ values of the individual oscillators it can be concluded that the soft modes $j=1$ are always in or close to the slow modulation limit. Accordingly, the

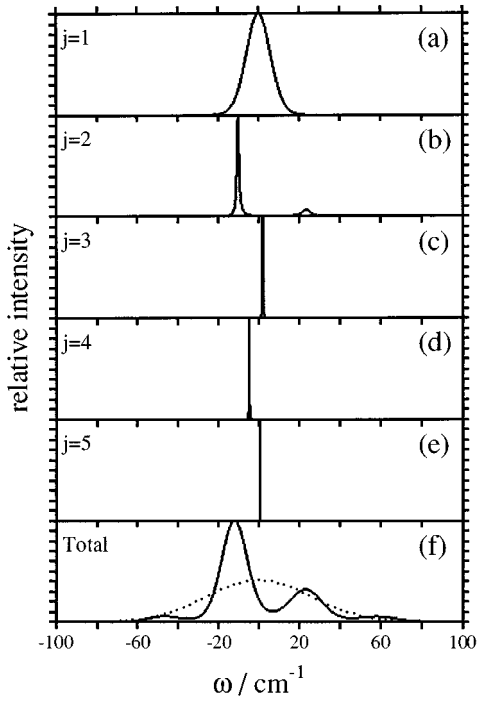

FIG. 4. The optical line shapes of the oscillators of the perylene·Ar_{14} cluster at 30 K using the simplified spectral line shape model and the $\{\omega_j,\Delta_j,\gamma_j\}$ parameters listed in Table I. For comparison the corresponding Gaussian (of the same dispersion value) has been added as a dotted curve in panel (f). In panel (a) the corresponding Gaussian (not shown) is almost congruent with the line shape; in panels (b)–(e) the Gaussians are too broad and weak for a meaningful representation on the intensity scale of the narrow line shapes.

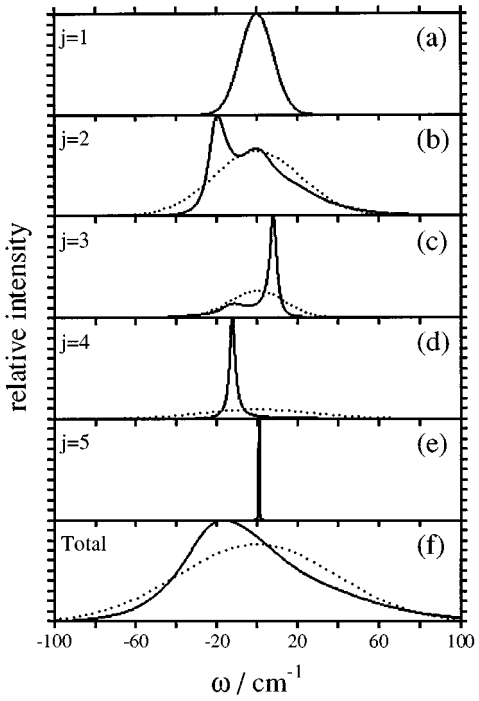

FIG. 5. The optical line shapes of the oscillators of the perylene·Ar_{279} cluster at 33 K using the simplified spectral line shape model and the $\{\omega_j, \Delta_j, \gamma_j\}$ parameters listed in Table I. The corresponding Gaussians (of the same dispersion values) have been added as dotted curves in panels (b)–(d) and (f). In panel (a) the Gaussian is not to be seen because of the congruence with the line shape; in panel (e) the Gaussian is too broad and weak to be visible on the scale of the narrow line shape.

linewidths Γ_1 obtained in the model calculations are close to the values $\Gamma_{\text{slow}}=2.355\Delta_1$, and the line shapes are almost congruent with Gaussians. The finite frequency oscillators are mostly in the fast modulation limit, as their $\gamma_j\tau_j$ values are much larger than 1 due to the low Δ_j^2/ω_j^2 ratios. Typical examples are exhibited for the $N=14$ cluster in Figs. 4(c)–4(e). The linewidths Γ_j come close to the $\Gamma_{\text{fast}}=2\gamma_j\kappa_j\Delta_j^2/(\omega_j^2+\gamma_j^2)$ values. Only oscillator 2, Fig. 4(b), tends somewhat towards the borderline between the fast modulation and the progression limit, forming the onset of a vibrational progression. The oscillators $j=2,3$ of the $N=279$ cluster at 33 K are exceptions among the studied finite frequency oscillators of this cluster type. The $j=2$ oscillator is in the domain between the slow modulation limit and a vibrational progression: the line shape, Fig. 5(b), starts to show a vibrational progression, but is not far from a Gaussian. The $j=3$ oscillator is a borderline case between the fast modulation and the progression limit, as also indicated by a $\gamma_j\tau_j$ value of 2.3. The line shape shows the $n=-1$ and the $n=0$ bands; the most intense peak is Lorentzianlike.

As discussed in Sec. III, one important effect of the cooperative action of all oscillators is the shortening of the total exponential decay times τ_{tot} with respect to the individual decay times τ_j and consequently a shift of all oscillators towards the slow modulation limit (the fast modulation limit→the progression limit→the slow modulation limit). This becomes apparent when comparing the $\omega_j\tau_j$ and $\gamma_j\tau_j$ values with the corresponding $\omega_j\tau_{\text{tot}}$ and $\gamma_j\tau_{\text{tot}}$ values. All soft modes, also of the $N=279$ cluster, get into the slow modulation limit. The finite frequency components are still in the fast modulation limit or are moved to the progression case. However, their small $\kappa_j\Delta_j^2/\omega_j^2$ ratios allow for not more than $n=2$ transitions.

The line broadening is almost quantitatively determined by the modes in the slow modulation limit.[13,14] Modes in the fast modulation or in the progression limit almost do not contribute because of the term ω_j^2 in the denominators, Eqs. (12) and (14). In perylene·Ar_N and tetracene-Ar_N heteroclusters, usually only the soft modes are in the slow modulation limit. It was previously found that the soft modes represent either cluster isomerizations or slow diffusive motions.[13,14] In the first case, the dispersion in the soft modes increases with the difference in the spectral shifts of the interconverting isomers. High dispersions in the soft modes and consequently broad spectral bands have been observed, in particular when the number of first-shell atoms changed upon cluster isomerization. Such processes in the cluster are accompanied by a strong temperature dependence of the linewidths. In the perylene·Ar_N clusters studied in this work, no cluster isomerization was observed. We note in particular that the structure of the first shell of the $N=279$ cluster was preserved up to 40 K, the highest considered temperature. It is therefore not surprising that the dispersion in the soft mode of the $N=279$ cluster at 33 K is not considerably higher (66.9 cm^{-2}) than that of the $N=14$ cluster (42.0 cm^{-2}). Instead, the soft modes pertain to the second class, denoted as slow diffusive motions, which are essentially low-frequency combination vibrations.

Unlike in other examples, the finite frequency oscillators $j=2,3$ ($\omega_j=21.4$ and -21.4 cm^{-1}) of the $N=279$ cluster at 33 K are also in the slow modulation limit. Accordingly, the total linewidth of 63.8 cm^{-1}, as obtained from the sum of the dispersions of three oscillators, is in very good agreement with the value of 66.2 cm^{-1} of the ''exact'' simulation, Table II.

B. The Xe($^1S_0\rightarrow{}^3P_1$) extravalence excitation of $XeAr_N$ heteroclusters

The Xe($^1S_0\rightarrow{}^3P_1$) Rydberg transition of $XeAr_N$ heteroclusters[17–20] constitutes another type of absorption spectra being characterized also by low vibrational frequencies but with much larger differences between the ground and excited electronic state potentials than in aromatic molecule–Ar heteroclusters. Figures 6 and 7 show the classical power spectra averaged over 20 trajectories, and the optical line shapes of the $N=12$ and the $N=199$ cluster at 20 K. The simulations[15] were carried out using Lennard-Jones 6-12 potentials for the electronic ground state and an exp-6 potential for the excited state Xe–Ar interactions.[48] The temporal length of each trajectory was 330 ps, the sampling interval of the energy gap function 5 fs for the $N=12$ and 10 fs for the $N=199$ cluster. The Xe atom is located at the center of both clusters. In the $N=12$ cluster, the Xe atom is surrounded by one closed shell of Ar atoms, where the sym-

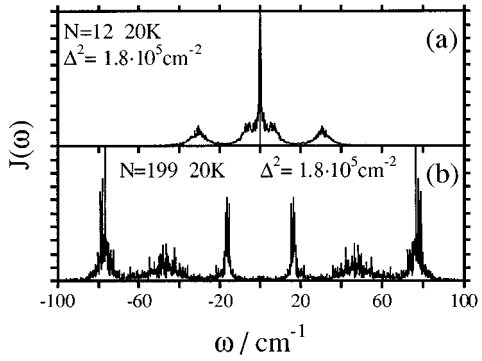

FIG. 6. The classical energy gap power spectra at 20 K (a) of the $XeAr_{12}$ and (b) of the $XeAr_{199}$ cluster. The total dispersion Δ^2 is indicated in each panel.

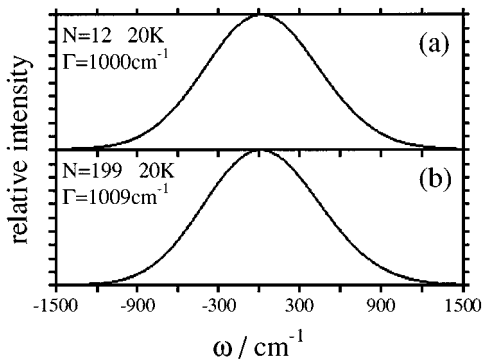

FIG. 7. The optical line shapes (a) of the $XeAr_{12}$ and (b) of the $XeAr_{199}$ cluster at 20 K obtained by the spectral density method. The center of each spectrum constitutes the origin of the energy axis, disregarding the different average gap values $\langle U \rangle$. The homogeneous linewidths Γ (FWHM) are indicated in each panel.

metry is icosahedral. The $N=199$ cluster consists of three shells, two closed icosahedral shells and a third incomplete outer shell.

The $\{\omega_j, \Delta_j, \gamma_j\}$ parameters extracted from the power spectra are listed in Table III. The oscillators carry dispersions, which are typically higher by 2 orders of magnitude than in the perylene·Ar_N clusters, manifesting the larger differences in the potential energy surfaces. The total dispersions of both $XeAr_N$ ($N=12,199$) clusters are similar, reflecting the fact that again interactions mainly with first shell Ar atoms contribute to the dispersion also for this extravalence electronic transition. The same applies to the spectral shift, which is, contrary to the perylene·Ar_N clusters, a blueshift. The considerable increase of the blue spectral shift from 2460 cm^{-1} of the $N=12$ to 7150 cm^{-1} of the $N=199$ cluster originates predominantly from a shortening of the first shell Xe–Ar distance caused by the stronger Xe–Ar bonding upon adding additional shells of Ar atoms.

The $\kappa_j\Delta_j^2/\omega_j^2$ values of the oscillators at positive frequencies range from 10 to 10^3. However, the corresponding optical line shapes of the single oscillators are Gaussians rather than very extensive vibrational progressions, as the oscillators are, according to the $\omega_j\tau_j$ and $\gamma_j\tau_j$ values, in the slow modulation limit. The absence of progressions can also be related to the high $\kappa_j\Delta_j^2/\omega_j^2$ values. In the progression limit the vibronic bands are Lorentzian, where for small n the linewidth, Eq. (14), is dominated by the term $2\gamma_j\kappa_j\Delta_j^2/\omega_j^2$. Therefore, the ratio $\kappa_j\Delta_j^2/\omega_j^2$ does not only determine the extension of a progression, but can be also considered as a magnification factor of the linewidth, leading to coalescence of the vibronic bands in the case of $XeAr_N$ clusters. In other words, the high $\kappa_j\Delta_j^2/\omega_j^2$ values require extremely small γ_j values in order not to coalesce to a Gaussian, which may be expected for di- and triatomic systems with a sparse vibrational level structure, where IVR rates are small. In correspondence to the quantum mechanical picture, the increase of the line broadening caused by the dispersion $\kappa_j\Delta_j^2$ can be interpreted as an accelerated decay of the initial wave packet subjected to an altered potential after the electronic excitation.

The power spectrum of the $N=12$ cluster has also a very intense soft mode, unlike the $N=199$ cluster, in which the shell structure is preserved at 20 K. The strong soft mode of the $N=12$ cluster originates from reversible wetting–nonwetting transitions, where the Xe surface is partially bared of Ar atoms, a process which is accompanied by a

TABLE III. The parametrization of the power spectra of $XeAr_N$ clusters and some derived quantities.

Spectrum	Osc. j	ω_j (cm^{-1})	Δ_j^2 (cm^{-2})	γ_j (cm^{-1})	κ_j	$\kappa_j\Delta_j^2/\omega_j^2$	τ_j (ps)	$\omega_j\tau_j$	$\gamma_j\tau_j$	$\omega_j\tau_{tot}$	$\gamma_j\tau_{tot}$
$N=12$, 20 K	1	0	44 540	0.7	1		0.033	0	$4.0\cdot10^{-3}$	0	$2.2\cdot10^{-3}$
	2	6.2	31 410	2.0	1.216	994	0.033	$4\cdot10^{-2}$	$1.3\cdot10^{-2}$	$1.9\cdot10^{-2}$	$6.3\cdot10^{-3}$
	3	−6.2	31 410	2.0	0.784	641	0.041	$5\cdot10^{-2}$	$1.6\cdot10^{-2}$	$1.9\cdot10^{-2}$	$6.3\cdot10^{-3}$
	4	31.0	31 140	3.0	1.803	58	0.025	0.14	$1.4\cdot10^{-2}$	$9.7\cdot10^{-2}$	$9.4\cdot10^{-3}$
	5	−31.0	31 140	3.0	0.197	6.4	0.091	0.53	$5.2\cdot10^{-2}$	$9.7\cdot10^{-2}$	$9.4\cdot10^{-3}$
	Total		179 700[a]				0.016				
$N=199$, 20 K	1	0	2 137	1.5	1		0.16	0	$4.5\cdot10^{-3}$	0	$4.7\cdot10^{-3}$
	2	16.4	19 240	1.0	1.529	109	0.041	0.13	$8.0\cdot10^{-3}$	$5.1\cdot10^{-2}$	$3.1\cdot10^{-3}$
	3	−16.4	19 240	1.0	0.471	34	0.075	0.23	$1.4\cdot10^{-2}$	$5.1\cdot10^{-2}$	$3.1\cdot10^{-3}$
	4	48.1	30 730	5.7	1.939	26	0.025	0.23	$2.7\cdot10^{-2}$	0.15	$1.8\cdot10^{-2}$
	5	−48.1	30 730	5.7	0.061	0.81	0.94	8.5	1.01	0.15	$1.8\cdot10^{-2}$
	6	77.5	34 810	5.7	1.992	12	0.025	0.36	$2.7\cdot10^{-2}$	0.24	$1.8\cdot10^{-2}$
	Total		184 100[a]				0.016				

[a]The total dispersion contains contributions of additional oscillators, which have not been parametrized.

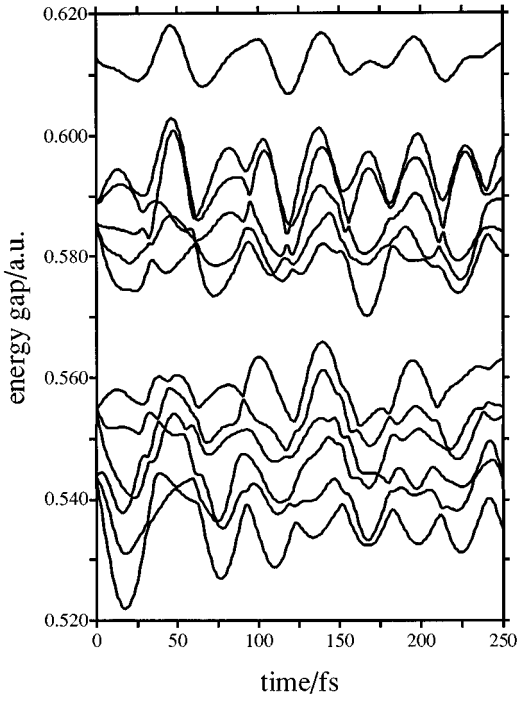

FIG. 8. The 12 energy gaps of the Li_4F_4 cubic cluster in the $2p$ valence region of fluorine within the first 250 fs of the simulation. The degeneracy at $t=0$ reflects the initially chosen T_d nuclear configuration. The temperature is 200 K.

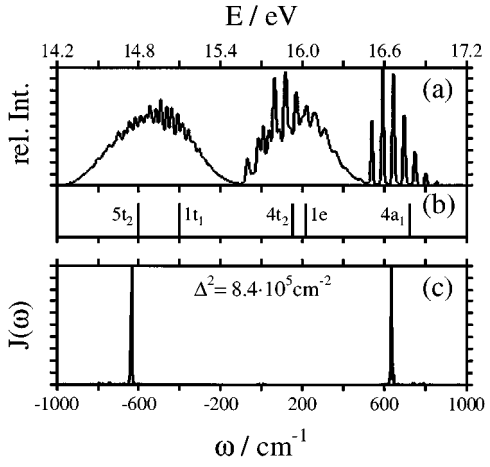

FIG. 9. (a) The total line shape of the Li_4F_4 cubic cluster at 200 K as the superposition of the 12 subspectra in the $2p$ valence region of fluorine. (b) A stick spectrum of the negative MO energies at the Li_4F_4 cube equilibrium nuclear configuration. (c) The energy gap power spectrum of the $4A_1$ ionization.

strong variation of the energy gap function. At 30 K (not considered in this work), a transition to a surface state takes place and the soft mode dominates the power spectrum.

When acting cooperatively, all oscillators get into the slow modulation limit. The slow modulation formula applied to the total dispersions yields linewidths of 999 and 1011 cm^{-1} for the $N=12$ and $N=199$ cluster, respectively, in excellent agreement with the values 1000 and 1009 cm^{-1} of the ''exact'' simulation.

C. The photoelectron spectrum of the Li_4F_4 cubic cluster

The photoelectron (PE) spectra of the Li_4F_4 cubic cluster (point group T_d) has been recently simulated using *ab initio* molecular dynamics (AIMD) simulations evaluating the forces on the nuclei at the Hartree–Fock SCF level.[16] The energy gap function $U(t)$ is given by the vertical ionization energy along the trajectory on the ground electronic state potential energy hypersurface. The ionization energies were calculated at the Koopmans level as the negative energies of the molecular orbitals (MOs).

Li_4F_4 has 24 doubly occupied MOs, the 12 highest are in the $2p$ valence region of fluorine. These MOs lie within a narrow energy range of less than 2 eV and therefore all have to be considered in a simulation of the total line shape. Figure 8 exhibits the 12 corresponding energy gaps for the first 250 fs at a temperature of 200 K. Since the spectral density method in its present version is based on a two-level model, the 12 ionizations had to be approximated by 12 independent two-level systems. The total line shape is then obtained by a superposition of the 12 individual subspectra, where the individual average energy gap values $\langle U \rangle$ of the subspectra determine their position on the absolute energy axis. In addition to the crudeness of an independent treatment of the energy gaps, the spectrum may be affected by strong nonadiabatic effects, which can be expected from the avoided crossings of the energy gap functions (Fig. 8). We therefore focus our discussion on the line shape of the $4A_1$ ionization (corresponding to the uppermost energy gap in Fig. 8), which is energetically more separated.

The total line shape is shown in Fig. 9 together with a stick spectrum of the negative MO energies of the cube T_d structure. The $4A_1$ ionization gives rise to a pronounced and well-resolved vibrational progression centered at 16.7 eV. The vibronic bands and their assignments are summarized in Table IV. The power spectrum, Fig. 9(c), is dominated by the two oscillators at ± 636 cm^{-1}, in accord with the spacing of the progression. The oscillators must be assigned to the $1A_1$ normal mode (harmonic vibrational frequency:[16] 646

TABLE IV. The spectral features of the simulated line shape of the $4A_1$ ionization band of the Li_4F_4 cubic cluster at 200 K.

ω (cm^{-1})[a]	Γ (cm^{-1})	Rel. int.[b]	Rel. int.[c]	Assignment n[d]
0	134	≡1	1.00	0
635	134	1.88	1.88	1
1273	138	1.82	1.78	2
1908	138	1.16	1.12	3
2547	142	0.56	0.53	4
3182	150	0.22	0.20	5
3820	154	0.07	0.06	6

[a]Band position relative to the position of the electronic origin, 16.5 eV.
[b]Relative intensity of the vibronic band from the area under the vibronic band.
[c]Expected relative intensity according to expression (11).
[d]Assignment to a vibronic transition n of the $1A_1$ (636 cm^{-1}) progression according to expression (11).

TABLE V. The parametrization of the power spectra of the $4A_1$ energy gap of the Li_4F_4 cluster at 200 K and some derived quantities.

Osc. j	ω_j (cm^{-1})	Δ_j^2 (cm^{-2})	γ_j (cm^{-1})	κ_j	$\kappa_j\Delta_j^2/\omega_j^2$	τ_j (ps)	$\omega_j\tau_j$	$\gamma_j\tau_j$	$\omega_j\tau_{tot}$	$\gamma_j\tau_{tot}$
1	11	759	2.2	1.039	6.52	0.27	0.57	0.11	0.22	$4.4\cdot10^{-2}$
2	−11	759	2.2	0.961	6.03	0.29	0.59	0.12	0.22	$4.4\cdot10^{-2}$
3	20	601	1.4	1.070	1.61	1.38	5.1	0.36	0.39	$2.8\cdot10^{-2}$
4	−20	601	1.4	0.930	1.40	1.77	6.5	0.47	0.39	$2.8\cdot10^{-2}$
5	27	146	1.6	1.096	0.22	13.7	69	4.2	0.54	$3.2\cdot10^{-2}$
6	−27	146	1.6	0.904	0.18	14.9	76	4.5	0.54	$3.2\cdot10^{-2}$
7	34	158	3.2	1.120	0.15	10.3	65	6.2	0.68	$6.4\cdot10^{-2}$
8	−34	158	3.2	0.880	0.12	13.2	83	7.9	0.68	$6.4\cdot10^{-2}$
9	636	383 200	2.2	1.980	1.88	0.83	99	0.34	12.8	$4.4\cdot10^{-2}$
Total		840 500[a]				0.11				

[a]The total dispersion contains contributions from additional oscillators, which have not been parametrized.

cm^{-1}), which is a breathing mode mainly of the lithium atoms. The parameters extracted from the power spectrum are given in Table V. The power spectrum contains also contributions below 50 cm^{-1} from combination vibrations, which are too weak to be seen in Fig. 9(c).

Expanding the energy gap U in a power series of an elongation Q_μ of a normal mode μ up to the linear term in Q_μ, where the expansion is carried out at the ground electronic state equilibrium nuclear configuration Q_0

$$U(Q_\mu)=U(Q_0)+\left(\frac{\partial U}{\partial Q_\mu}\right)_{Q_0}\cdot(Q_\mu-Q_0)+\cdots \tag{19}$$

and U is given by the corresponding negative orbital energy ϵ, the dispersion Δ_j^2 of oscillator j is expected to be proportional to $(\partial\epsilon/\partial Q_\mu)^2$. The numerically obtained $(\partial\epsilon/\partial Q_\mu)^2$ value assumes only an appreciable value for the $1A_1$ mode. We mention in passing that the $1A_1$ mode is active for all energy gaps; some energy gaps exhibit also the $2A_1$ mode (harmonic vibrational frequency:[16] 373 cm^{-1}).

From the $\omega_j\tau_j$, $\gamma_j\tau_j$, $\gamma_j\tau_{tot}$, and $\omega_j\tau_{tot}$ values derived and given in Table V it can be stated that the $1A_1$ normal mode is in the progression limit as an isolated oscillator, as well as when considering the combined action of all oscillators. With increasing the absolute frequency of the isolated combination vibrations they exhibit the three cases of the slow modulation limit, the progression limit and the fast modulation limit. In the combined action of all oscillators they always correspond to the slow modulation limit.

The line broadening is almost exclusively determined by the low-frequency combination vibrations, although the sum of their dispersion, 3328 cm^{-2}, forms only a small fraction of the total value, $8.4\cdot10^5$ cm^{-2}. The low-frequency dispersion results in a FWHM of 136 cm^{-1} (slow modulation limit), in good agreement with the simulated linewidth of 134–154 cm^{-1}, Table IV. In comparison, the contribution of the $1A_1$ normal mode to the linewidth Γ of the $n=0$ transition is small, 8.3 cm^{-1} [Eq. (14)].

The subspectra of the other energy gaps show a similar behavior. The normal modes are always in the progression limit, but in some cases the line broadening due to the low-frequency combination vibrations drives the entire line shape into the slow modulation limit, leading to a coalescence of the progression to an unresolved Gaussian line shape. Although a more realistic description of the line shape of Li_4F_4 (incorporating nonadiabatic effects) may modify the features, the phenomenon of the coalescence of a progression into a Gaussian line shape by low-frequency modes is expected to be general and to be exhibited in other systems. Such a behavior is different from the $XeAr_N$ clusters, where all the main oscillators are in the slow modulation limit per se. But in either case, the width of the resulting total line shape is given by applying the slow modulation formula to the entire dispersion of the energy gap.

V. CONCLUSIONS

Using a simplified model for the energy gap power spectrum, we have derived an analytical expression for the transition dipole autocorrelation function in the framework of the spectral density formalism. The derived expressions allowed for a comparative discussion of the line shapes previously simulated using the spectral density method: (i) The absorption line shapes of the electronic origin of the perylene $S_0\rightarrow S_1(\pi\pi^*)$ transition in perylene$\cdot Ar_N$ clusters; (ii) the absorption line shapes of the $Xe(^1S_0\rightarrow{}^3P_1)$ extravalence transition in $XeAr_N$ clusters; and (iii) the photoelectron spectrum of the Li_4F_4 cubic cluster. The spectra provide examples for weak, unresolved and extensive vibrational progressions.

To make contact between our simulations and experimental reality, it is useful to address some of the implications of the results and analysis. Regarding the perylene$\cdot Ar_N$ clusters the detailed predictions of the vibronic fine structure will be very useful when it will become possible to sort out isomer-specific spectra of these systems, which can be experimentally accomplished by hole burning methods.[46,47,49–51] The simulations of related systems, e.g., naphthalene$\cdot Ar_N$ ($N=1$–15)[8,9] and tetracene$\cdot Ar_N$ ($N=1$–50),[12,37] and the comparison of spectral shifts and line broadening with experiment, have already proven the reliability of our approach. Further detailed comparison between the simulations of the vibronic structure and experiment will be useful to improve the intermolecular potentials for these systems. Regarding the spectra of the $XeAr_N$ clusters (which correspond to the slow modulation limit and exhibit Gauss-

ian line shapes where all vibronic structure is washed out) the simulated line shapes are in excellent agreement with the experimental spectroscopic data.[15] For the photoelectron spectra of the Li_4F_4 cluster, no experimental information is currently available. The appearance of the vibrational progression of the $1A_1$ mode in the $4A_1$ ionization spectrum will confirm the simulations. The lack of a resolved vibrational progression could have two reasons: (i) the role of nonadiabatic effects also for the $4A_1$ ionization and (ii) high temperature effects, as simulations at 500 K showed the coalescence of the vibrational progression. For a meaningful analysis of the photoelectron spectra of Li_4F_4 the simulations have to be extended to consider also the ladder and the ring isomers of this cluster.[16,52] Already at this stage a wealth of interesting information emerges for several classes of molecular and ionic clusters.

In the simplified line shape model, each peak (''oscillator'') j of the energy gap power spectrum is described by a Lorentzian, characterized by a frequency ω_j of its peak maximum, the dispersion Δ_j^2 (the area under the curve) and the half width at half maximum γ_j. Δ_j^2 expresses the difference between the shape of the ground and the excited electronic state potential energy hypersurfaces in the region accessible by the classical trajectories. γ_j reflects the effect of intracluster vibrational energy redistribution (IVR).

The line shape model has three limiting cases: (i) The fast modulation limit, where only the electronic origin is exhibited as a single Lorentzian band; (ii) the limit of a vibrational progression (''progression limit''), where each vibronic band is Lorentzian; and (iii) the slow modulation limit with a Gaussian line shape. While limit (i) and (iii) are known from the work pioneered by Kubo,[32,33] limit (ii) is new.

Which of the limiting cases is approached by a single oscillator depends on the parameters $\omega_j, \Delta_j, \gamma_j$, and on the derived exponential decay time τ_j of the transition dipole autocorrelation function. With decreasing τ_j the line shape passes the three limiting cases in the order fast modulation limit→progression limit→slow modulation limit. The *entire* line shape, which is the entity to be compared with an experimental spectrum or a spectrum from an ''exact'' simulation, is given by the cooperative action of all oscillators. When acting cooperatively, each oscillator contributes to the line broadening, shortening the exponential decay time τ_{tot} of the total transition dipole autocorrelation function. A simple relation between τ_{tot} and the individual τ_j and the corresponding parameters ω_j, Δ_j, and γ_j was found only in the fast modulation limit. An oscillator with a sufficiently short exponential decay time can drive the entire line shape into the slow modulation limit.

The criteria for the realization of the three limiting cases are (i) fast modulation limit: $\gamma_j\tau \gg 1$, (ii) progression limit: $\omega_j\tau \gg 2\pi$ and $\gamma_j\tau \ll 1$, (iii) slow modulation limit: $\omega_j\tau \ll 1$ and $\gamma_j\tau \ll 1$, where τ is given either by τ_j or τ_{tot}, depending whether one considers a single oscillator or the interplay of all oscillators. Single oscillators can meet these conditions for the following parameter constellations: (i) fast modulation limit: $\omega_j \gg \Delta_j, \gamma_j$, (ii) progression limit: $\omega_j \approx \Delta_j \gg \gamma_j$, (iii) slow modulation limit: $\Delta_j \gg \omega_j, \gamma_j$. With growing the Δ_j^2/ω_j^2 ratio the extension of a vibrational progression but also the line broadening increases, shifting the oscillator towards the slow modulation limit. The parameter constellations lead to the following classification:

(i) Small intermolecular vibrational frequencies (<50 cm^{-1}) and even smaller Δ_j values, which result in small Δ_j^2/ω_j^2 values ($\ll 1$) for the main oscillators (oscillators carrying the major part of the dispersion). This case is represented by perylene$\cdot \mathrm{Ar}_N$ clusters. The main oscillators are in the fast modulation limit and are driven into the progression limit when acting cooperatively, mainly by the soft modes (low-frequency combination vibrations or cluster isomerizations), which also make up the dominant contribution to the line broadening. The small Δ_j^2/ω_j^2 values of the main oscillators allow only for an onset of a vibrational progression.

(ii) Small intermolecular vibrational frequencies (<50 cm^{-1}) and large dispersions, resulting in large $\Delta_j^2/\omega_j^2 \gg 1$ values. This is the case of the XeAr_N clusters. Instead of achieving very extensive vibrational progressions, the excessive line broadening leads to the slow modulation limit of each single main oscillator. In this sense, the Gaussian line shape can be thought of as an unresolved vibrational progression. The entire dispersion contributes to the line broadening.

(iii) Larger vibrational frequencies (at least several hundred wave numbers) and large dispersions, so that the Δ_j^2/ω_j^2 values of the main oscillators are of the order of 1 and give rise to extensive vibrational progressions. This is the situation of the photoelectron spectrum of the Li_4F_4 cluster, which can be considered to be a typical example for a large number of molecular systems with a bound electronically excited state. It is unlikely that the dispersion can assume such high values that the Δ_j^2/ω_j^2 ratio reaches values $\gg 1$ as in the case of XeAr_N clusters. The simplified line shape model can be used to assign the vibronic bands of the progression on the basis of the intensities. However, as the Li_4F_4 example has shown, the moderate Δ_j^2/ω_j^2 values are no guarantee for resolved progressions. As in case (i), the major part of the line broadening originates from low-frequency combination vibrations. In some cases the line broadening, due to the low-frequency combination vibrations, is so large that the slow modulation limit is reached. In this case, the Gaussian spans the entire progression. It is difficult to predict the magnitude of line broadening of the combination vibrations on the basis of qualitative arguments.

It is most desirable to predict line shapes by some simple rules of thumb. Although the entire line shape is given by the cooperative action of all oscillators, in most cases it may prove sufficient to predict the overall character of a line shape (the appearance and extension or nonappearance of a vibrational progression, Gaussian or Lorentzian line shape) by examining the parameter constellation of the main oscillators. The three types of example spectra discussed in this work provide a valuable orientation.

ACKNOWLEDGMENTS

A.H. is indebted to Professor J. Sauer for his interest and support of this work. This research was supported by the Deutsche Forschungsgemeinschaft (Sonderforschungsbereich 377).

[1] L. E. Fried and S. Mukamel, Phys. Rev. Lett. **66**, 2340 (1991).
[2] L. E. Fried and S. Mukamel, J. Chem. Phys. **96**, 116 (1992).
[3] S. Mukamel, J. Chem. Phys. **77**, 173 (1982).
[4] S. Mukamel, Phys. Rep. **93**, 1 (1982).
[5] J. Sue, Y. J. Yan, and S. Mukamel, J. Chem. Phys. **85**, 462 (1986).
[6] R. Islampour and S. Mukamel, Chem. Phys. Lett. **107**, 239 (1984).
[7] R. Islampour and S. Mukamel, J. Chem. Phys. **80**, 5487 (1984).
[8] T. Troxler and S. Leutwyler, Ber. Bunsenges. Phys. Chem. **96**, 1246 (1992).
[9] T. Troxler and S. Leutwyler, J. Chem. Phys. **99**, 4363 (1993).
[10] P. Parneix, F. G. Amar, and Ph. Brechignac, Z. Phys. D **26**, 217 (1993).
[11] P. Parneix, P. Hermine, F. G. Amar, and Ph. Brechignac, in *Physics and Chemistry of Finite Systems: From Clusters to Crystals*, edited by P. Jena, S. N. Khanna, and B. K. Rao, NATO ASI Series C (Kluwer, Dordrecht, 1992), Vol. I, p. 453.
[12] A. Heidenreich and J. Jortner, Z. Phys. D **26**, 377 (1993).
[13] A. Heidenreich and J. Jortner, Isr. J. Chem. **33**, 467 (1993).
[14] A. Heidenreich, D. Bahatt, N. Ben-Horin, U. Even, and J. Jortner, J. Chem. Phys. **100**, 6300 (1994).
[15] A. Goldberg, A. Heidenreich, and J. Jortner, J. Phys. Chem. **99**, 2662 (1995).
[16] A. Heidenreich and J. Sauer, Z. Phys. D **35**, 279 (1995).
[17] T. Möller, Z. Phys. D **20**, 1 (1991).
[18] J. Wörmer and T. Möller, Z. Phys. D **20**, 39 (1991).
[19] M. Lengen, M. Joppien, R. Müller, J. Wörmer, and T. Möller, Phys. Rev. Lett. **68**, 2362 (1992).
[20] M. Lengen, M. Joppien, R. von Pietrowski, and T. Möller, Chem. Phys. Lett. **229**, 362 (1994).
[21] E. J. Heller, Acc. Chem. Res. **14**, 368 (1981).
[22] E. J. Heller, J. Chem. Phys. **68**, 2066 (1978)
[23] E. J. Heller, in *Potential Energy Surface and Dynamics Calculations*, edited by D. G. Truhlar (Plenum, New York, 1981), p. 103.
[24] R. Schinke, *Photodissociation Dynamics* (Cambridge University, Cambridge 1993).
[25] J. G. Saven and J. L. Skinner, J. Chem. Phys. **99**, 4391 (1993).
[26] J. G. Saven and J. L. Skinner, in *Reaction Dynamics in Clusters and Condensed Phases*, edited by J. Jortner, R. D. Levine, and B. Pullman (Kluwer, Dordrecht, 1994), p. 461.
[27] L. E. Fried and S. Mukamel, Adv. Chem. Phys. **84**, 435 (1993).
[28] J. Jortner and N. Ben-Horin, J. Chem. Phys. **98**, 9346 (1993).
[29] *Mode Selectivity in Unimolecular Reactions*, Special Issue, edited by J. Manz and C. S. Parmenter, Chem. Phys. **139**, 1 (1989).
[30] *Mode Selective Chemistry*, edited by J. Jortner, R. D. Levine, and B. Pullman (Kluwer, Dordrecht, 1991).
[31] A. H. Zewail, *Femtochemistry* (World Scientific, Singapore, 1994), and references therein.
[32] R. Kubo and Y. Toyozawa, Prog. Theoret. Phys. **13**, 160 (1955).
[33] R. Kubo, Adv. Chem. Phys. **15**, 101 (1969).
[34] G. E. Uhlenbeck and L. S. Ornstein, Phys. Rev. **36**, 823 (1930).
[35] G. N. Robertson and J. Jarwood, Chem. Phys. **32**, 267 (1978).
[36] W. G. Rothschild, J. Soussen-Jacob, J. Bessiere, and J. Vincent-Geisse, J. Chem. Phys. **79**, 3002 (1983).
[37] A. Heidenreich and J. Jortner (unpublished).
[38] N. Ben-Horin, U. Even, J. Jortner, and S. Leutwyler, J. Chem. Phys. **97**, 5296 (1992).
[39] N. Ben-Horin, D. Bahatt, U. Even, and J. Jortner, J. Chem. Phys. **97**, 6011 (1992).
[40] P. Dauber-Osguthorpe and D. J. Osguthorpe, J. Comput. Chem. **14**, 1259 (1993).
[41] E. Shalev, N. Ben-Horin, U. Even, and J. Jortner, J. Chem. Phys. **95**, 3147 (1991).
[42] N. Ben-Horin, U. Even, and J. Jortner, J. Chem. Phys. **97**, 5988 (1992).
[43] F. Fillaux, Chem. Phys. Lett. **114**, 384 (1985)
[44] B. Fourmann, C. Jouvet, A. Tramer, J. M. Le Bars, and Ph. Millie, Chem. Phys. **92**, 25 (1985).
[45] M. A. Doxtader, E. A. Mangle, A. K. Bhattacharya, S. M. Cohen, and M. R. Topp, Chem. Phys. **101**, 413 (1986).
[46] S. A. Wittmeyer and M. R. Topp, Chem. Phys. Lett. **163**, 261 (1989); **171**, 29 (1990).
[47] S. A. Wittmeyer and M. R. Topp, J. Phys. Chem. **95**, 4627, 5017 (1991).
[48] I. Messing, B. Raz, and J. Jortner, J. Chem. Phys. **66**, 2239 (1977).
[49] B. Dick, E. Zinghar, and Y. Haas, Chem. Phys. Lett. **187**, 571 (1991)
[50] R. Jankowiak, J. M. Hayes, and G. J. Small, Chem. Rev. **93**, 1471 (1993)
[51] M. Orrit, J. Bernard, and R. I. Personov, J. Phys. Chem. **97**, 10256 (1993)
[52] C. Ochsenfeld and R. Ahlrichs, Ber. Bunsenges. Phys. Chem. **98**, 34 (1994).